Local Elastic and Geometric Stiffness Matrices for the Shell Element Applied in cFEM

Dávid Visy[1], Sándor Ádány[1*]

Abstract

In this paper local elastic and geometric stiffness matrices of a shell finite element are presented and discussed. The shell finite element is a rectangular plane element, specifically designed for the so-called constrained finite element method. One of the most notable features of the proposed shell finite element is that two perpendicular (in-plane) directions are distinguished, which is resulted in an unusual combination of otherwise classic shape functions. An important speciality of the derived stiffness matrices is that various options are considered, which allows the user to decide how to consider the through-thickness stress-strain distributions, as well as which second-order strain terms to consider from the Green-Lagrange strain matrix. The derivations of the stiffness matrices are briefly summarized then numerical examples are provided. The numerical examples illustrate the effect of the various options, as well as they are used to prove the correctness of the proposed shell element and of the completed derivations.

Keywords:

constrained Finite Element Method, elastic and geometric stiffness matrices

1 Introduction

Thin-walled structural members, e.g., cold-formed steel members, have complicated behaviour. If subjected to compressive stresses, it is the stability behaviour which is most likely governing. Instability might occur in various forms, these forms are typically classified as global buckling (e.g., flexural buckling of a column or lateral-torsional buckling of a beam), distortional buckling and local buckling (e.g., local plate buckling of a compressed plate, or shear buckling of a plate in shear, or web crippling of a transversally loaded web of a plate girder, etc.). In practical situations these buckling classes rarely appear in isolation, but in combination with one another.

The classification into global (G), distortional (D), local (L) and other (O) modes is used in capacity prediction, too, and appears either implicitly or explicitly in current design standards for cold-formed steel, see [1,2]. Though the knowledge of pure buckling modes and the values of the associated critical loads are essential in the design of thin-walled members, still there are practical cases when decomposition of the behaviour into the mode spaces (e.g., pure G, pure D, or pure L modes) has not been possible. Till lately there have been two available methods with general modal decomposition features: the generalized beam theory (GBT), see e.g. [3–5], and the constrained finite strip method (cFSM), see e.g. [6–11]. Though both methods can handle important practical cases, both have limitations, for example members with cross-section changes or members with holes are not covered at all.

Very recently a novel method is proposed. The proposed method follows the logic of cFSM, however, discretization is used in both the transverse and longitudinal direction, that is finite elements are used instead of finite strips, therefore, the new method can be described as constrained finite element method (cFEM).

cFEM uses a novel shell finite element, specifically designed for the method. The new element keeps the transverse interpolation functions of finite strips as in [6–11], however, the longitudinal interpolation functions are changed from trigonometric functions (or function series) to classic polynomials. It is found, however, that the polynomial longitudinal interpolation

[1]Budapest University of Technology and Economics, Budapest, Hungary
[*]Corresponding author, email: sadany@epito.bme.hu

functions must be specially selected in order to be able to perform modal decomposition similarly as in cFSM. This requires an unusual combination of otherwise well-known shape functions. The proposed interpolation functions and their derivation can be found in detail in [12].

The cFEM has first been applied in [13–15]. Since cFEM method is using shell finite elements, various engineering problems can be solved. If the modal features are to be utilized, a highly regular mesh is necessary. This required regularity of the mesh means a practical limitation, but otherwise the method is general: first- and second-order static analysis as well as dynamic analyses can be performed, for arbitrary loading and boundary conditions. Holes can easily be handled, too, once they fit into the regular mesh.

In this paper the local stiffness matrices (e.g., elastic and geometric stiffness matrices) of the proposed shell element are discussed. Since the finite element is rectangular, the matrices can be derived analytically. Previous studies highlighted the importance of some details of the derivations. As shown e.g. in [16], three factors must carefully be considered: (a) whether the through-thickness stress-strain variation is considered or disregarded in deriving the elastic stiffness matrix, (b) whether the through-thickness stress-strain variation is considered or disregarded in deriving the geometric stiffness matrix, and (c) which second-order strain terms are considered in the derivation of the geometric stiffness matrix. As previous studies showed [16–18], various analytical and numerical methods apply various options, therefore it is useful to have the stiffness matrices in various options which makes the here discussed cFEM directly comparable to many other methods. Moreover, numerical results of cFEM suggests that ability to select the various second-order strain terms in arbitrary combinations leads to a deeper understanding of the behaviour as well as makes it possible to fine-tune the (buckling) analysis of thin-walled members. Therefore, the aim of this paper is to present the derivation of the local elastic and geometric stiffness matrices in various options, then illustrate the applicability of the proposed shell elements. The numerical examples, first, prove the correctness of the proposed shell element and that of the completed derivations. Moreover, the examples illustrate the – sometimes significant – effect of the various options.

2 Derivation of the stiffness matrices
2.1 General

Since the proposed cFEM is evolved from cFSM, the new shell element inherits the transverse interpolation functions from FSM, while the longitudinal interpolation functions are changed from trigonometric functions to polynomials. However, in order to be able to exactly satisfy the constraining criteria for mode decomposition, the new polynomial longitudinal shape functions must have some important characteristics. These key features are as follows: (i) the transverse in-plane

displacements must be interpolated by using the same shape functions as used for the out-of-plane displacements, (ii) the longitudinal base function for $u(x, y)$ must be the first derivative of the longitudinal base function for $v(x, y)$. For the basic notations see Fig. 1. Moreover, it is desirable to provide $C^{(1)}$ continuous interpolation for the out-of-plane displacements (which is useful for defining various practical end restraints).

Thus, the distinction of longitudinal and transverse directions is essential. Though unusual in shell finite elements, the element proposed for cFEM distinguishes the two perpendicular directions, as given by Fig. 1. Finally, the proposed element has 30 DOF: 6 for u, 8 for v and 16 for w. Each corner node has 7 DOF (1 for u, 2 for v, and 4 for w), while there are two additional nodes at $(x, y) = (a/2, 0)$ and $(x, y) = (a/2, b)$ with one DOF per node for the u displacement. The DOF and shape functions are illustrated in Fig. 2.

The derivations of the stiffness matrices follow the typical steps. However, various options are considered, as follows. Both the elastic and geometric stiffness matrices are derived with assuming linear or constant (i.e., approximate) stress-strain variation through the thickness of the element. Moreover, since in cFEM all the possible in-plane stresses/strains are reasonable to consider (i.e., longitudinal and transverse normal stress/strain and shear stress/strain), there are altogether 3×3 second-order strain terms, in accordance with the 2D Green-Lagrange strain matrix; the geometric stiffness matrix is derived so that any of the 9 second-order strain terms can be considered or disregarded.

2.2 Overview of the derivations

The vector of general displacement field, u, is approximated with the matrix of shape functions, N, and the vector of the nodal displacements, d, as:

$$u = \begin{bmatrix} u(x, y, z) \\ v(x, y, z) \\ w(x, y, z) \end{bmatrix} = Nd \qquad (1)$$

The matrix of shape functions can be written in the following form:

$$N = \begin{bmatrix} N_u & 0 & 0 & -z\dfrac{\partial N_w}{\partial x} & -z\dfrac{\partial N_{\vartheta x}}{\partial x} & -z\dfrac{\partial N_{\vartheta y}}{\partial x} & -z\dfrac{\partial N_{\vartheta xy}}{\partial x} \\ 0 & N_v & N_{\vartheta z} & -z\dfrac{\partial N_w}{\partial y} & -z\dfrac{\partial N_{\vartheta x}}{\partial y} & -z\dfrac{\partial N_{\vartheta y}}{\partial y} & -z\dfrac{\partial N_{\vartheta xy}}{\partial y} \\ 0 & 0 & 0 & N_w & N_{\vartheta x} & N_{\vartheta y} & N_{\vartheta xy} \end{bmatrix}$$

$$(2)$$

where the shape functions for approximation of in-plane displacements are N_u, N_v and $N_{\vartheta z}$, while for approximation of out-of-plane displacement is N_w, $N_{\vartheta x}$, $N_{\vartheta y}$ and $N_{\vartheta xy}$, as:
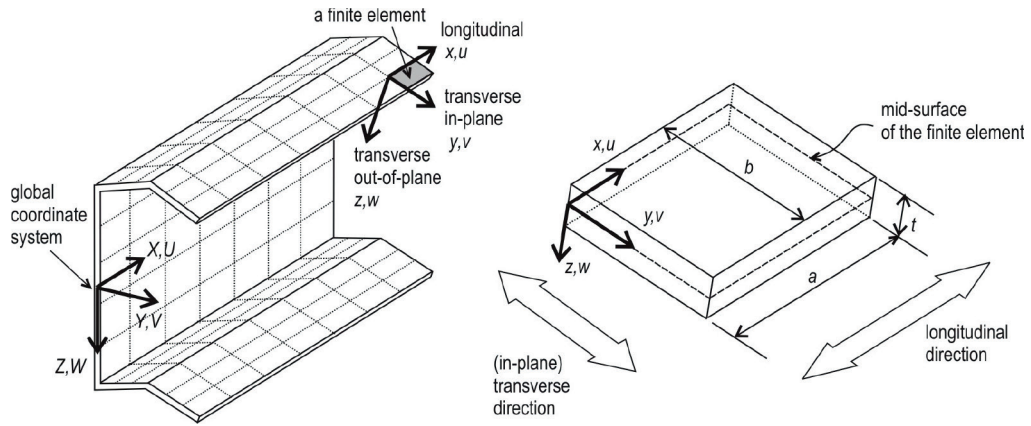
Fig. 1 FEM discretization, coordinates, basic notations
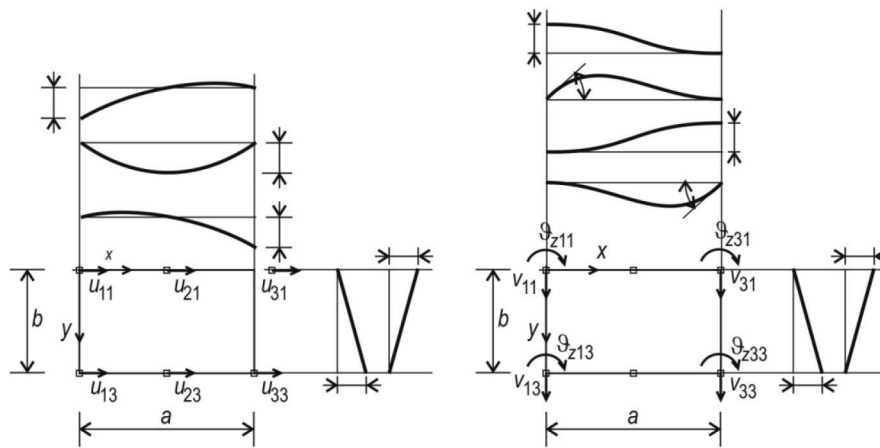
(a) in-plane displacements
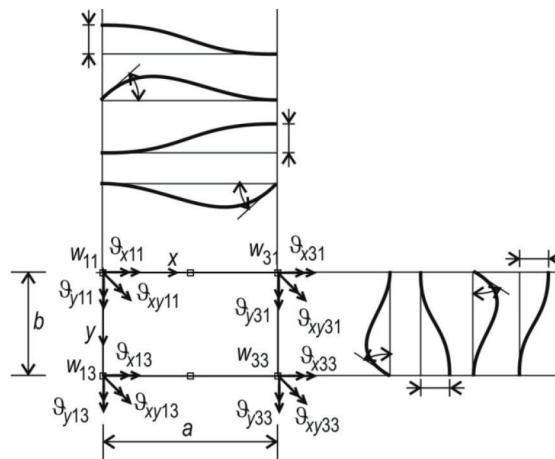
(b) out-of-plane displacements

Fig. 2 Nodal DOF of the proposed shell finite element

$$N_u = \begin{bmatrix} N_{x,1}^{(2)} N_{y,1}^{(1)} & N_{x,1}^{(2)} N_{y,2}^{(1)} & N_{x,2}^{(2)} N_{y,1}^{(1)} & N_{x,2}^{(2)} N_{y,2}^{(1)} & N_{x,3}^{(2)} N_{y,1}^{(1)} & N_{x,3}^{(2)} N_{y,2}^{(1)} \end{bmatrix} \tag{3}$$

$$N_v = \begin{bmatrix} N_{x,1}^{(3)} N_{y,1}^{(1)} & N_{x,1}^{(3)} N_{y,2}^{(1)} & N_{x,3}^{(3)} N_{y,1}^{(1)} & N_{x,3}^{(3)} N_{y,2}^{(1)} \end{bmatrix} \tag{4}$$

$$N_{\vartheta z} = \begin{bmatrix} N_{x,2}^{(3)} N_{y,1}^{(1)} & N_{x,2}^{(3)} N_{y,2}^{(1)} & N_{x,4}^{(3)} N_{y,1}^{(1)} & N_{x,4}^{(3)} N_{y,2}^{(1)} \end{bmatrix} \tag{5}$$

$$N_w = \begin{bmatrix} N_{x,1}^{(3)} N_{y,1}^{(3)} & N_{x,1}^{(3)} N_{y,3}^{(3)} & N_{x,3}^{(3)} N_{y,1}^{(3)} & N_{x,3}^{(3)} N_{y,3}^{(3)} \end{bmatrix} \tag{6}$$

$$N_{\vartheta x} = \begin{bmatrix} N_{x,1}^{(3)} N_{y,2}^{(3)} & N_{x,1}^{(3)} N_{y,4}^{(3)} & N_{x,3}^{(3)} N_{y,2}^{(3)} & N_{x,3}^{(3)} N_{y,4}^{(3)} \end{bmatrix} \tag{7}$$

$$N_{\vartheta y} = \begin{bmatrix} -N_{x,2}^{(3)} N_{y,1}^{(3)} & -N_{x,2}^{(3)} N_{y,3}^{(3)} & -N_{x,4}^{(3)} N_{y,1}^{(3)} & -N_{x,4}^{(3)} N_{y,3}^{(3)} \end{bmatrix} \tag{8}$$

$$N_{\vartheta xy} = \begin{bmatrix} -N_{x,2}^{(3)} N_{y,2}^{(3)} & -N_{x,2}^{(3)} N_{y,4}^{(3)} & -N_{x,4}^{(3)} N_{y,2}^{(3)} & -N_{x,4}^{(3)} N_{y,4}^{(3)} \end{bmatrix} \tag{9}$$

In Eqs. (3) to (9) linear, second and third order functions are used for the interpolation. In Eqs. (10) and (11) the second and third order functions are shown for x direction, while in Eqs. (12) and (13) the linear and third order functions are shown for y direction interpolation. The bracketed numbers in the superscript means the order of the functions.

$$N_{x,1}^{(2)} = 1 - \frac{3x}{a} + \frac{2x^2}{a^2}, \quad N_{x,2}^{(2)} = \frac{4x}{a} - \frac{4x^2}{a^2}$$
$$\text{and} \quad N_{x,3}^{(2)} = -\frac{x}{a} + \frac{2x^2}{a^2} \tag{10}$$

$$N_{x,1}^{(3)} = 1 - \frac{3x^2}{a^2} + \frac{2x^3}{a^3}, \quad N_{x,2}^{(3)} = x - \frac{2x^2}{a} + \frac{x^3}{a^2},$$
$$N_{x,3}^{(3)} = \frac{3x^2}{a^2} - \frac{2x^3}{a^3} \quad \text{and} \quad N_{x,4}^{(3)} = -\frac{x^2}{a} + \frac{x^3}{a^2} \tag{11}$$

$$N_{y,1}^{(1)} = 1 - \frac{y}{b} \quad \text{and} \quad N_{y,2}^{(1)} = \frac{y}{b} \tag{12}$$

$$N_{y,1}^{(3)} = 1 - \frac{3y^2}{b^2} + \frac{2y^3}{b^3}, \quad N_{y,2}^{(3)} = y - \frac{2y^2}{b} + \frac{y^3}{b^2},$$
$$N_{y,3}^{(3)} = \frac{3y^2}{b^2} - \frac{2y^3}{b^3} \quad \text{and} \quad N_{y,4}^{(3)} = -\frac{y^2}{b} + \frac{y^3}{b^2} \tag{13}$$

The vector of the nodal displacements can be written in the following form:

$$d = \begin{bmatrix} d_u & d_v & d_{\vartheta z} & d_w & d_{\vartheta x} & d_{\vartheta y} & d_{\vartheta xy} \end{bmatrix}^{\mathrm{T}} \tag{14}$$

where the sub-vectors contain separately the different degrees of freedoms for the nodes, as:

$$d_u = \begin{bmatrix} u_{11} & u_{13} & u_{21} & u_{23} & u_{31} & u_{33} \end{bmatrix} \tag{15}$$

$$d_v = \begin{bmatrix} v_{11} & v_{13} & v_{31} & v_{33} \end{bmatrix} \tag{16}$$

$$d_{\vartheta z} = \begin{bmatrix} \vartheta_{z,11} & \vartheta_{z,13} & \vartheta_{z,31} & \vartheta_{z,33} \end{bmatrix} \tag{17}$$

$$d_w = \begin{bmatrix} w_{11} & w_{13} & w_{31} & w_{33} \end{bmatrix} \tag{18}$$

$$d_{\vartheta x} = \begin{bmatrix} \vartheta_{x,11} & \vartheta_{x,13} & \vartheta_{x,31} & \vartheta_{x,33} \end{bmatrix} \tag{19}$$

$$d_{\vartheta y} = \begin{bmatrix} \vartheta_{y,11} & \vartheta_{y,13} & \vartheta_{y,31} & \vartheta_{y,33} \end{bmatrix} \tag{20}$$

$$d_{\vartheta xy} = \begin{bmatrix} \vartheta_{xy,11} & \vartheta_{xy,13} & \vartheta_{xy,31} & \vartheta_{xy,33} \end{bmatrix} \tag{21}$$

The strain vector, ϵ, can be expressed by an operator matrix, L, and the vector of nodal displacement field, u (see Eq. (1)), as:

$$\epsilon = \begin{bmatrix} \epsilon_x(x,y,z) \\ \epsilon_y(x,y,z) \\ \gamma_{xy}(x,y,z) \end{bmatrix} = Lu = LNd = Bd \tag{22}$$

where the operator matrix is:

$$L = \begin{bmatrix} \dfrac{\partial}{\partial x} & 0 & 0 \\ 0 & \dfrac{\partial}{\partial y} & 0 \\ \dfrac{\partial}{\partial y} & \dfrac{\partial}{\partial x} & 0 \end{bmatrix} \tag{23}$$

The stress vector, σ, can be expressed with the material matrix, E, and the strain vector, ϵ, as:

$$\sigma = \begin{bmatrix} \sigma_x(x,y,z) \\ \sigma_y(x,y,z) \\ \tau_{xy}(x,y,z) \end{bmatrix} = E\epsilon = EBd \tag{24}$$

where the material matrix, assuming linear elastic orthotropic material, is:

$$E = \begin{bmatrix} E_{11} & E_{12} & 0 \\ E_{21} & E_{22} & 0 \\ 0 & 0 & G \end{bmatrix} = \begin{bmatrix} \dfrac{E_x}{1-\nu_{xy}\nu_{yx}} & \dfrac{\nu_{yx}E_x}{1-\nu_{xy}\nu_{yx}} & 0 \\ \dfrac{\nu_{xy}E_y}{1-\nu_{xy}\nu_{yx}} & \dfrac{E_y}{1-\nu_{xy}\nu_{yx}} & 0 \\ 0 & 0 & G \end{bmatrix} \tag{25}$$

Since the method is intended to be applicable for geometrically nonlinear analysis (e.g., linear buckling analysis), nonlinear strains must be considered. This is completed here by using the second-order terms of Green-Lagrange strains, as:

$$\epsilon_x^{II} = \frac{1}{2}\left[\left(\frac{\partial u}{\partial x}\right)^2 + \left(\frac{\partial v}{\partial x}\right)^2 + \left(\frac{\partial w}{\partial x}\right)^2\right] \tag{26}$$

$$\epsilon_y^{II} = \frac{1}{2}\left[\left(\frac{\partial u}{\partial y}\right)^2 + \left(\frac{\partial v}{\partial y}\right)^2 + \left(\frac{\partial w}{\partial y}\right)^2\right] \tag{27}$$

$$\gamma_{xy}^{II} = \begin{bmatrix} \frac{1}{2}\frac{\partial u}{\partial x}\frac{\partial u}{\partial y} + \frac{1}{2}\frac{\partial v}{\partial x}\frac{\partial v}{\partial y} + \frac{1}{2}\frac{\partial w}{\partial x}\frac{\partial w}{\partial y} + \frac{1}{2}\frac{\partial u}{\partial y}\frac{\partial u}{\partial x} \\ + \frac{1}{2}\frac{\partial v}{\partial y}\frac{\partial v}{\partial x} + \frac{1}{2}\frac{\partial w}{\partial y}\frac{\partial w}{\partial x} \end{bmatrix} \tag{28}$$

which can be expressed with the matrix of shape functions and the vector of the nodal displacements using Eqs. (2) and (14), as:

$$\epsilon_x^{II} = \frac{1}{2}d^T\frac{\partial N^T}{\partial x}\frac{\partial N}{\partial x}d = \frac{1}{2}d^T G_x{}^T G_x d \tag{29}$$

$$\epsilon_y^{II} = \frac{1}{2}d^T\frac{\partial N^T}{\partial y}\frac{\partial N}{\partial y}d = \frac{1}{2}d^T G_y{}^T G_y d \tag{30}$$

$$\gamma_{xy}^{II} = d^T\left[\frac{1}{2}\frac{\partial N^T}{\partial x}\frac{\partial N}{\partial y} + \frac{1}{2}\frac{\partial N^T}{\partial y}\frac{\partial N}{\partial x}\right]d = \frac{1}{2}d^T\left[G_x{}^T G_y + G_y{}^T G_x\right]d \tag{31}$$

The total potential energy, Đ, can be calculated from the internal and the external potential (i.e., the negative of the work), as:

$$\Pi = \Pi_{int} + \Pi_{ext} \tag{32}$$

The internal potential energy, Đ, can be expressed using Eqs. (22) and (24), as:

$$\Pi_{int} = \frac{1}{2}\int_V \epsilon^T \sigma dV = \frac{1}{2}\int_V \epsilon^T E \epsilon dV$$
$$= \frac{1}{2}d^T\left[\int_V B^T EB dV\right]d = \frac{1}{2}d^T k_e d \tag{33}$$

The external potential can be written as follows, using Eqs. (29)–(31), as:

where the $\sigma_{x,0}$, $\sigma_{y,0}$ and $\tau_{xy,0}$ functions are the initial stress functions calculated from the results (nodal displacements, d_0) of a previous linear or nonlinear static analysis, as:

$$\sigma_0 = \begin{bmatrix} \sigma_{x,0}(x,y,z) \\ \sigma_{y,0}(x,y,z) \\ \tau_{xy,0}(x,y,z) \end{bmatrix} = E\epsilon_0 = EB d_0 \tag{35}$$

In Eq. (33) the elastic stiffness matrix, while in Eq. (34) the geometric stiffness matrix appears, both can be derived in the following definite integral form, which result 30-by-30 matrices:

$$k_e = \int_{-t/2}^{t/2}\int_0^b\int_0^a B^T EB dx dy dz \tag{36}$$

$$k_g = \int_{-t/2}^{t/2}\int_0^b\int_0^a \begin{bmatrix} \sigma_{x,0}G_x{}^T G_x + \sigma_{y,0}G_y{}^T G_y + \tau_{xy,0} \\ \left(G_x{}^T G_y + G_y{}^T G_x\right) \end{bmatrix} dx dy dz \tag{37}$$

2.3 The elastic stiffness matrix

The elastic stiffness matrix appears in the calculation of internal potential energy (see Eq. (33)). Though the steps shown in Section 2 are always valid, simplifications in the formulae are possible and sometimes applied, namely in performing the integration to calculate the elastic stiffness matrix (see Eq. (36)). Two options are used in the practice: the variation of strains and stresses through the thickness can be considered or disregarded, which latter case corresponds to neglecting the bending energy. It also means that the elastic stiffness matrix has two different versions, one is the $k_e^{(0)}$ matrix (see Eq. (38)) when trough-thickness stress-strain variation is neglected, the other is the $k_e^{(1)}$ matrix (see Eq. (39)), when through-thickness stress-strain variation is considered. (Note, in case of the formula in Eq. (38) B should be considered with its mean value, i.e. with substituting $z = 0$.)

$$k_e^{(0)} = t\int_0^b\int_0^a B^T EB dx dy \tag{38}$$

$$k_e^{(1)} = \int_{-t/2}^{t/2}\int_0^b\int_0^a B^T EB dx dy dz \tag{39}$$

$$\Pi_{ext} = -\int_V\left(\sigma_{x,0}\epsilon_x^{II} + \sigma_{y,0}\epsilon_y^{II} + \tau_{xy,0}\gamma_{xy}^{II}\right)dV$$
$$= -\frac{1}{2}d^T\left[\int_V\left[\sigma_{x,0}G_x{}^T G_x + \sigma_{y,0}G_y{}^T G_y + \tau_{xy,0}\left(G_x{}^T G_y + G_y{}^T G_x\right)\right]dV\right]d \tag{34}$$
$$= -\frac{1}{2}d^T\left(k_{g,x} + k_{g,y} + k_{g,xy}\right)d = -\frac{1}{2}d^T k_g d$$

The substitution and subsequent integration leads to closed-formed solutions for the 30-by-30 matrices. The elements of the matrices are really large, therefore the exact matrices are not shown in the paper, only the non-zero and zero sub-matrices. In the following equations 0 denotes zero matrices with the necessary sizes. If the through-thickness stress-strain variation is neglected, the elastic stiffness matrix is the following:

$$k_e^{(0)} = \begin{bmatrix} k_{e,11}^{(0)} & 0 \\ 0 & 0 \end{bmatrix} \qquad (40)$$

where the one non-zero $k_{e,11}^{(0)}$ term is a 14-by-14 matrix. The $k_e^{(0)}$ matrix corresponds to that finite element, which has only membrane stiffness, but does not have bending stiffness.

If the through-thickness stress-strain variation is considered, the elastic stiffness matrix can be calculated from $k_e^{(0)}$ with an additional matrix, $\Delta k_e^{(1)}$, as:

$$k_e^{(1)} = k_e^{(0)} + \Delta k_e^{(1)} \qquad (41)$$

where the additional matrix is

$$\Delta k_e^{(1)} = \begin{bmatrix} 0 & 0 \\ 0 & \Delta k_{e,22}^{(1)} \end{bmatrix} \qquad (42)$$

in which the one non-zero $\Delta k_{e,22}^{(1)}$ term is a 16-by-16 matrix. The $\Delta k_e^{(1)}$ matrix corresponds to that finite element, which has only bending stiffness, but does not have membrane stiffness, while the $k_e^{(1)}$ matrix corresponds to that case, when the finite element has both membrane and bending stiffness.

2.4 The geometric stiffness matrix

The geometric stiffness matrix appears in the calculation of the external potential energy (see Eq. (34)). As it is mentioned in Section 3, simplifications in the formulae can be applied, which statement is valid also in case of geometric stiffness matrix (see Eq. (37)). Simplification is possible at two steps, namely: (i) in performing the integration in geometric stiffness matrix, and (ii) in the definition of second-order strains.

In performing the integration, also two options are used in the practice: the through thickness integration can be neglected or considered. The first case is widely used especially for thin-walled members, where the effect of the variation through the thickness is negligible (see Eq. (43)), while the second one is the mathematically precise one (see Eq. (44)). (In case of the formula in Eq. (43), all functions should be considered with their mean values, i.e. with substituting $z = 0$.)

$$k_g^{(0)} = t \int_0^b \int_0^a \begin{bmatrix} \sigma_{x,0} G_x{}^T G_x + \sigma_{y,0} G_y{}^T G_y + \\ \tau_{xy,0} \left(G_x{}^T G_y + G_y{}^T G_x \right) \end{bmatrix} dxdy \qquad (43)$$

$$k_g^{(1)} = \int_{-t/2}^{t/2} \int_0^b \int_0^a \begin{bmatrix} \sigma_{x,0} G_x{}^T G_x + \sigma_{y,0} G_y{}^T G_y + \\ \tau_{xy,0} \left(G_x{}^T G_y + G_y{}^T G_x \right) \end{bmatrix} dxdydz \qquad (44)$$

If the through thickness integration is neglected, the $k_g^{(0)}$ matrix can be written in the following separated form:

$$k_g^{(0)} = k_{g,x}^{(0)} + k_{g,y}^{(0)} + k_{g,xy}^{(0)} \qquad (45)$$

where $k_{g,x}^{(0)}$, $k_{g,y}^{(0)}$ and $k_{g,xy}^{(0)}$ represent the three partial matrices calculated from second-order strain terms ϵ_x^{II}, ϵ_y^{II} and γ_{xy}^{II} (see Eqs. (26), (27), (28) and (34)). Furthermore, as the three second-order strain terms can be separated (e.g. in case of ϵ_x^{II} to $(\partial u / \partial x)^2$, $(\partial v / \partial x)^2$, and $(\partial w / \partial x)^2$ terms), the partial matrices can be separated as well in the following forms:

$$k_{g,x}^{(0)} = k_{g,ux}^{(0)} + k_{g,vx}^{(0)} + k_{g,wx}^{(0)} \qquad (46)$$

$$k_{g,y}^{(0)} = k_{g,uy}^{(0)} + k_{g,vy}^{(0)} + k_{g,wy}^{(0)} \qquad (47)$$

$$k_{g,xy}^{(0)} = k_{g,uxy}^{(0)} + k_{g,vxy}^{(0)} + k_{g,wxy}^{(0)} \qquad (48)$$

In case of the geometric stiffness matrix the substitution and subsequent integration also leads to closed-formed solutions for the 30-by-30 matrices. Without real through-thickness integration, i.e., by using Eq. (43), it leads to $k_g^{(0)}$ as follows:

$$k_g^{(0)} = \begin{bmatrix} k_{g,11}^{(0)} & 0 & 0 \\ 0 & k_{g,22}^{(0)} & 0 \\ 0 & 0 & k_{g,33}^{(0)} \end{bmatrix} \qquad (49)$$

where

$$k_{g,11}^{(0)} = k_{g,ux,11}^{(0)} + k_{g,uy,11}^{(0)} + k_{g,uxy,11}^{(0)} \qquad (50)$$

$$k_{g,22}^{(0)} = k_{g,vx,22}^{(0)} + k_{g,vy,22}^{(0)} + k_{g,vxy,22}^{(0)} \qquad (51)$$

$$k_{g,33}^{(0)} = k_{g,wx,33}^{(0)} + k_{g,wy,33}^{(0)} + k_{g,wxy,33}^{(0)} \qquad (52)$$

where $k_{g,11}^{(0)}$ is a 6-by-6, $k_{g,22}^{(0)}$ is an 8-by-8, and $k_{g,33}^{(0)}$ is a 16-by-16 matrix, and the subscript of the matrices correspond to the displacement derivative, e.g., the matrix with the *ux* subscript comes from the $(\partial u / \partial x)^2$ term of the Green-Lagrange matrix, etc.

As mentioned, the matrix elements can be expressed analytically, by long mathematical expressions. For example, the (1,1) element of $k_g^{(0)}$ is expressed by:

$$k_{g,ux,11}^{(0)}(1,1) = -\frac{13}{180}E_{12}t\vartheta_{z,11} + \frac{13}{180}E_{12}t\vartheta_{z,13} + \frac{1}{36}E_{12}t\vartheta_{z,31} - \frac{1}{36}E_{12}t\vartheta_{z,33}$$
$$-\frac{5b}{4a^2}E_{11}tu_{11} - \frac{5b}{12a^2}E_{11}tu_{13} + \frac{4b}{3a^2}E_{11}tu_{21} + \frac{4b}{9a^2}E_{11}tu_{23} - \frac{b}{12a^2}E_{11}tu_{31} \tag{53}$$
$$-\frac{b}{36a^2}E_{11}tu_{33} - \frac{59}{90a}E_{12}tv_{11} + \frac{59}{90a}E_{12}tv_{13} - \frac{11}{90a}E_{12}tv_{31} + \frac{11}{90a}E_{12}tv_{33}$$

$$k_{g,uy,11}^{(0)}(1,1) = -\frac{a^2}{105b^2}E_{22}t\vartheta_{z,11} + \frac{a^2}{105b^2}E_{22}t\vartheta_{z,13} + \frac{a^2}{420b^2}E_{22}t\vartheta_{z,31} - \frac{a^2}{420b^2}E_{22}t\vartheta_{z,33}$$
$$-\frac{1}{6b}E_{21}tu_{11} - \frac{1}{6b}E_{21}tu_{13} + \frac{1}{5b}E_{21}tu_{21} + \frac{1}{5b}E_{21}tu_{23} - \frac{1}{30b}E_{21}tu_{31} - \frac{1}{30b}E_{21}tu_{33} \tag{54}$$
$$-\frac{13a}{105b^2}E_{22}tv_{11} + \frac{13a}{105b^2}E_{22}tv_{13} - \frac{a}{105b^2}E_{22}tv_{31} + \frac{a}{105b^2}E_{22}tv_{33}$$

$$k_{g,uxy,11}^{(0)}(1,1) = \frac{17}{90}Gt\vartheta_{z,11} + \frac{17}{180}Gt\vartheta_{z,13} - \frac{1}{18}Gt\vartheta_{z,31} - \frac{1}{36}Gt\vartheta_{z,33}$$
$$-\frac{1}{3b}Gtu_{11} + \frac{1}{3b}Gtu_{13} - \frac{1}{5b}Gtu_{21} + \frac{1}{5b}Gtu_{23} + \frac{1}{30b}Gtu_{31} - \frac{1}{30b}Gtu_{33} \tag{55}$$
$$-\frac{1}{5a}Gtv_{11} - \frac{1}{10a}Gtv_{13} + \frac{1}{5a}Gtv_{31} + \frac{1}{10a}Gtv_{33}$$

If through thickness integration is considered as in Eq. (44), the geometric stiffness matrix can be calculated from $k_g^{(0)}$ with additional matrices, as:

$$k_g^{(1)} = k_g^{(0)} + \Delta k_{g,x}^{(1)} + \Delta k_{g,y}^{(1)} + \Delta k_{g,xy}^{(1)} \tag{56}$$

where $\Delta k_{g,x}^{(1)}$, $\Delta k_{g,y}^{(1)}$ and $\Delta k_{g,xy}^{(1)}$ represent also the three partial additional matrices calculated from second-order strain terms ϵ_x^{II}, ϵ_y^{II} and γ_{xy}^{II}. The partial matrices can be separated as well in the following forms:

$$\Delta k_{g,x}^{(1)} = \Delta k_{g,ux}^{(1)} + \Delta k_{g,vx}^{(1)} + \Delta k_{g,wx}^{(1)} \tag{57}$$

$$\Delta k_{g,y}^{(1)} = \Delta k_{g,uy}^{(1)} + \Delta k_{g,vy}^{(1)} + \Delta k_{g,wy}^{(1)} \tag{58}$$

$$\Delta k_{g,xy}^{(1)} = \Delta k_{g,uxy}^{(1)} + \Delta k_{g,vxy}^{(1)} + \Delta k_{g,wxy}^{(1)} \tag{59}$$

If the through-thickness integration is performed as in Eq. (44), $k_g^{(1)}$ also can be expressed as:

$$k_g^{(1)} = k_g^{(0)} + \Delta k_g^{(1)} \tag{60}$$

The additional stiffness matrix takes the form as:

$$\Delta k_g^{(1)} = \begin{bmatrix} 0 & 0 & \Delta k_{g,13}^{(1)} \\ 0 & 0 & \Delta k_{g,23}^{(1)} \\ \Delta k_{g,13}^{(1)\,T} & \Delta k_{g,23}^{(1)\,T} & \Delta k_{g,33}^{(1)} \end{bmatrix} \tag{61}$$

where

$$\Delta k_{g,13}^{(1)} = \Delta k_{g,ux,13}^{(1)} + \Delta k_{g,uy,13}^{(1)} + \Delta k_{g,uxy,13}^{(1)} \tag{62}$$

$$\Delta k_{g,23}^{(1)} = \Delta k_{g,vx,23}^{(1)} + \Delta k_{g,vy,23}^{(1)} + \Delta k_{g,vxy,23}^{(1)} \tag{63}$$

$$\Delta k_{g,33}^{(1)} = \Delta k_{g,ux,33}^{(1)} + \Delta k_{g,uy,33}^{(1)} + \Delta k_{g,uxy,33}^{(1)} \\ + \Delta k_{g,vx,33}^{(1)} + \Delta k_{g,vy,33}^{(1)} + \Delta k_{g,vxy,33}^{(1)} \tag{64}$$

where $\Delta k_{g,13}^{(1)}$ is a 6-by-16, $\Delta k_{g,23}^{(1)}$ is an 8-by-16, and $\Delta k_{g,33}^{(1)}$ is a 16-by-16 matrix, and the subscript of the matrices correspond to the displacement derivative.

2.5 Stiffness matrices of a member

The global stiffness matrices of a member consists of multiple elements can be assembled using k_e and k_g. The matrices must be transformed from local to global coordinate system, then the global elastic and geometric stiffness matrices, K_e and K_g, can be compiled. Transformation of the stiffness matrices of element j follows from:

$$K_e^{(j)} = \Gamma^{(j)\,T} k_e^{(j)} \Gamma^{(j)} \tag{65}$$

and

$$K_g^{(j)} = \Gamma^{(j)\,T} k_g^{(j)} \Gamma^{(j)} \tag{66}$$

where $\Gamma^{(j)}$ is the 2D rotation matrix. The global stiffness matrices may be assembled as an appropriate summation of the local stiffness matrices for all the s elements:

$$K_e = \sum_{\substack{j=1..s \\ \text{assembly}}} K_e^{(j)} \tag{67}$$

and

$$K_g = \sum_{\substack{j=1..s \\ \text{assembly}}} K_g^{(j)} \tag{68}$$

3 Numerical studies
3.1 Verifications

First some examples are solved by both the newly proposed cFEM analyses and ANSYS shell FEM analyses [19]. Critical load and buckled shapes are calculated and compared. Two lipped channel sections are considered, with 200 mm depth, 40

or 100 mm wide flanges, 20 mm lip length and 2 mm of thickness. The member length is 1000 mm. The material is steel like isotropic material, but considered in two versions, one with $E = 200GPa$, $v = 0.3$, (therefore $G = 76.923GPa$), the other one with $E = 200GPa$ and $v = 0.0$ (therefore $G = 100GPa$). In all the cases the member is supported at the end sections in a locally and globally hinged manner.

Three types of loading are considered. In case of „compression" the member is in pure compression due to two opposite concentric axial forces (acting as uniformly distributed over the end sections). In case of "UDL" there is a uniformly distributed transverse loading acting at the junction of the web and one or both of the flanges. In case of "shear" there are forces acting along the edges of the web panel so that they produce (practically) pure shear stresses in the whole web.

In all these examples critical loads are calculated the member being either unconstrained when "all mode" is considered, or constrained to global modes („pure G") or to global plus shear mode („G+S"). In case of cFEM the constraining is realized by introducing the mechanical criteria (that lead to constraint matrices), essentially identically as in cFSM [6–18]. In case of ANSYS shell FE analysis the constraints are realized by rigid diaphragms, as discussed e.g. in [18].

Some buckled shapes are shown in Figs. 3-8. and the calculated critical loads (first modes, i.e., lowest critical values) are summarized in Table 1.
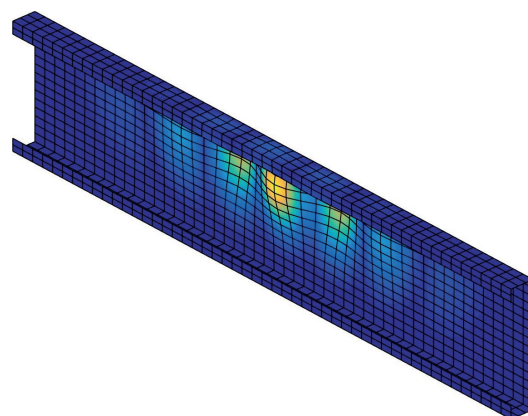
cFEM: F_{cr} = 99.8601 kN
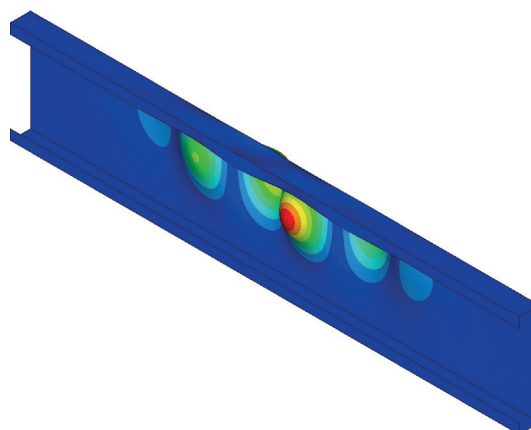
ANSYS: F_{cr} = 99.6041 kN

Fig. 3 C200-40-20-2, 1000 mm, $E = 200GPa$, $v = 0.3$, UDL on bottom, all mode

Table 1 Critical loads for the different cases in cFEM and ANSYS FEM

Section		Loading	Modes	cFEM	ANSYS
C200-40-20-2	0.3	UDL on top	all	69.6734	70.1583
C200-40-20-2	0.3	UDL on top & bottom	all	93.3895	93.1812
C200-40-20-2	0.3	UDL on bottom	all	99.8601	99.6041
C200-100-20-2	0.3	UDL on top	all	88.3214	88.5718
C200-100-20-2	0.3	UDL on top & bottom	all	108.4916	108.485
C200-100-20-2	0.3	UDL on bottom	all	118.9608	118.928
C200-40-20-2	0.3	shear	all	29.8280	29.7643
C200-100-20-2	0.3	shear	all	33.1738	33.2009
C200-40-20-2	0.3	compression	pure G	74.8342	72.938
C200-40-20-2	0.0	compression	pure G	294.4093	293.91
C200-100-20-2	0.3	compression	pure G	461.2501	–
C200-100-20-2	0.3	compression	G+S	438.5351	436.287
C200-100-20-2	0.0	compression	pure G	1307.428	–
C200-100-20-2	0.0	compression	G+S	1263.210	1255.83
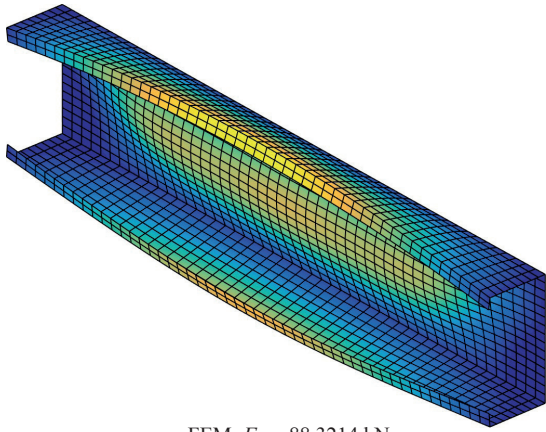
cFEM: F_{cr} = 88.3214 kN
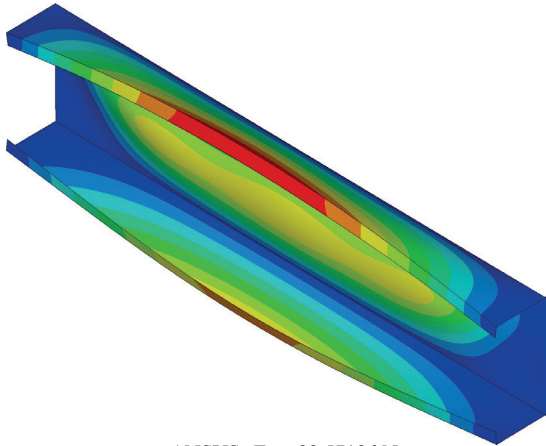
ANSYS: F_{cr} = 88.5718 kN

Fig. 4 C200-100-20-2, 1000 mm, $E = 200GPa$, $v = 0.3$, UDL on top, all mode
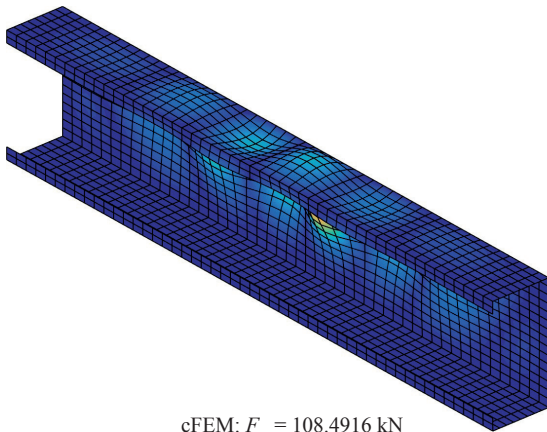
cFEM: F_{cr} = 108.4916 kN
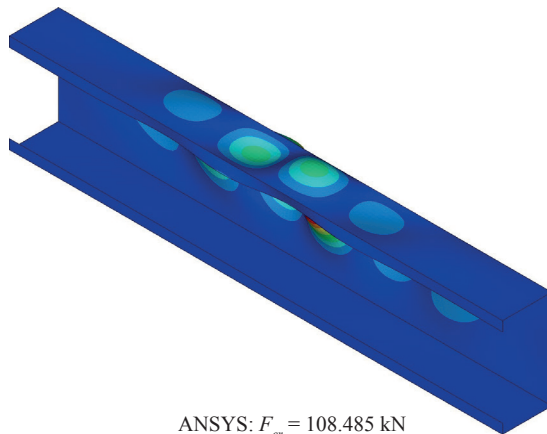
ANSYS: F_{cr} = 108.485 kN

Fig. 5 C200-100-20-2, 1000 mm, $E = 200GPa$, $v = 0.3$, UDL on top and bottom, all mode
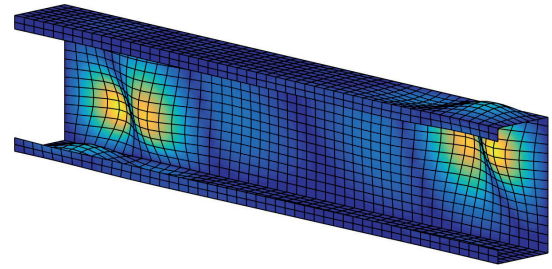
cFEM: F_{cr} = 33.1738 kN
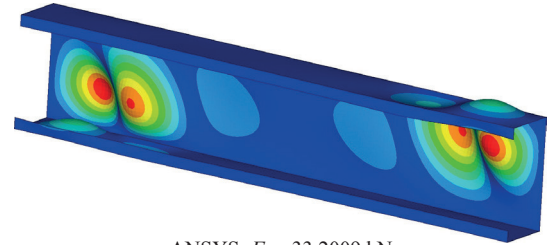
ANSYS: F_{cr} = 33.2009 kN

Fig. 6 C200-100-20-2, 1000 mm, $E = 200GPa$, $v = 0.3$, shear, all mode
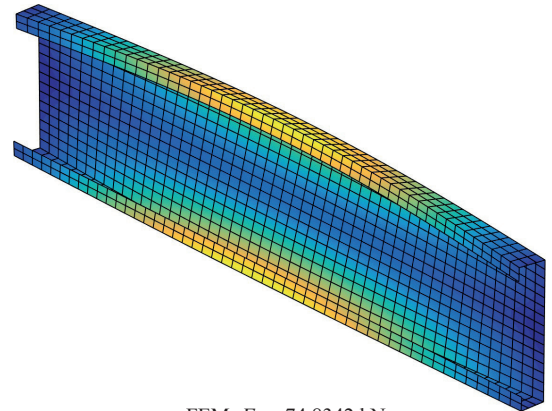
cFEM: F_{cr} = 74.8342 kN
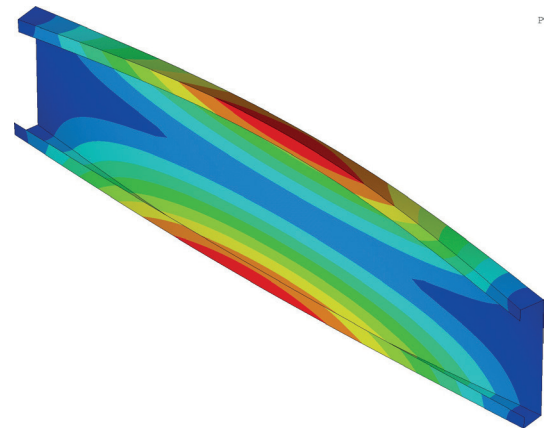
ANSYS: F_{cr} = 72.938 kN

Fig. 7 C200-40-20-2, 1000 mm, $E = 200GPa$, $v = 0.3$, compression, pure G
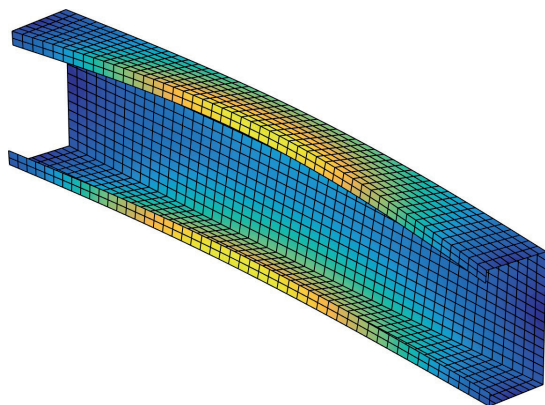
cFEM: F_{cr} = 1307.428 kN (with shear: F_{cr} = 1263.210 kN)
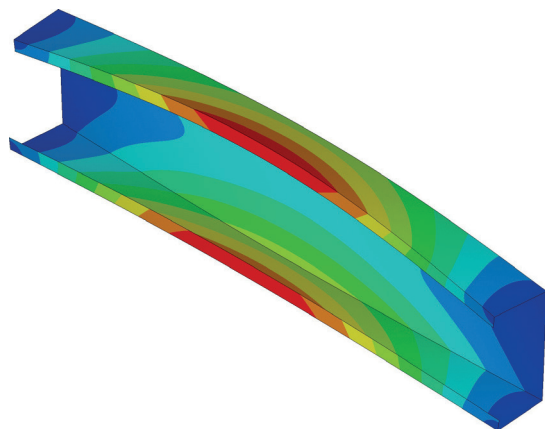
ANSYS: F_{cr} = 1255.83 kN

Fig. 8 C200-100-20-2, 1000 mm, $E = 200 GPa$, $v = 0.3$, compression, pure G

It can be concluded that the proposed new shell finite element leads to results practically identical to those from ANSYS shell FEM analysis in regular unconstrained cases. General constraints cannot be implemented in ANSYS, still, the mechanical criteria of global modes can reasonably well imitated by the application of rigid diaphragms, and once these diaphragms are used, the critical values of ANSYS coincide well with those from cFEM. It is also to observe, however, that the diaphragms themselves do not prevent the in-plane shear deformations, therefore, shear modes must also be considered in cFEM in order to achieve good coincidence in between ANSYS and cFEM.

3.2 Demonstration of the effect of longitudinal strain term

First the effect of longitudinal second-order strain term $(\partial u / \partial x)^2$ is demonstrated. The effect of this term on the global buckling of columns is discussed e.g. in [17, 18] in the context of finite strip method as well as analytical solutions. Moreover, the effect of this term is discussed in [20] with considering in-plane shear deformations. As already demonstrated, if this term is disregarded, the critical force tend to infinity as the member length approaches zero (like in Euler formula for flexural buckling), while if this term is considered, the critical force tends to a finite value. This finite critical stress value is

dependent on some other options, but it is close to the Young's modulus, if shear deformations are not considered.

In Tab. 2 major-axis flexural buckling critical stresses are summarized calculated for the 40-mm-wide lipped channel section (defined in Section 3.1) in pure compression with $v = 0.0$. The critical forces are calculated for various member lengths and in 4 options depending on whether the longitudinal strain term $(\partial u / \partial x)^2$ is considered or not, and whether the deformation are constrained into the pure G or to G + S mode spaces.

Table 2 Critical loads for the different longitudinal strain term options in cFEM

Length [mm]	$(\partial u / \partial x)^2$ neglected	$(\partial u / \partial x)^2$ considered	$(\partial u / \partial x)^2$ neglected	$(\partial u / \partial x)^2$ considered
Mode	pure G	pure G	G+S	G+S
20	27 635 675	198 566	74 604.6	74 350.8
50	4 421 793	191 348	72 721.9	71 876.0
100	1 105 430	169 361	68 814.9	66 577.0
200	276 354	116 030	57 584.3	53 460.1
500	44 216.5	36 211.0	27 443.7	25 189.4
1000	11 054.1	10 475.2	9 587.68	9 202.68
2000	2 763.53	2 725.87	2 661.72	2 628.02
5000	442.165	441.189	439.475	438.517

The results in Table 2 clearly show the importance of the $(\partial u / \partial x)^2$ in case of short members, especially when the analysis is constrained into the pure G space. It is to note that the first column of Tab. 2 is practically identical to the solution from the Euler-formula, while the other columns can be compared to analytical solutions from [20] or e.g to cFSM solutions.

3.3 Demonstration of the effect various second-order strain terms

The buckling types which are characterized by localized out-of-plane plate displacements can all be classified as „local buckling". In the structural engineering practice, however, these local buckling types are further categorized, and it is common to distinguish local-plate buckling, shear buckling or (web) crippling. This categorization is included in the modern design standards, too, see e.g. [1,2]. When talking about the buckling of a web of a plate girder, „plate buckling" is primarily due to longitudinal normal (compressive) stresses, "shear buckling" is due to shear stresses, while „web crippling" is due to transverse normal (compressive) stresses. In most of the practical situations these stresses appear simultaneously, therefore, the local buckling of a web is most probably due to the combination of various stress components, i.e., the buckling mode is most probably a combination of various local buckling types. However, since in the here-summarized derivations the effects of various second-order strain terms are separated, the various local buckling types can easily be separated.

To demonstrate the effect of various second-order strain terms, a lipped-channel beam is analysed. The beam is 600 mm long, having the C section with the 40 mm wide flanges. The beam is loaded by a transverse force at the middle of the beam, acting at the plane of the web in two positions: „top" or „bottom", depending on whether the transverse force is acting at the top or bottom flange. The load is a quasi-concentrated force, i.e. it is placed on the beam as a uniformly distributed loading with distribution length of 100 mm (so that the resultant would be 1 kN). The beam is simply supported at its two ends, just as in the previous examples.

The problem is solved in various options, depending on which stress components are considered or disregarded during the calculations. According to the local coordinate system of the applied shell element, 'sigx' is the longitudinal normal stress, 'sigy' is the transverse normal stress, while 'tauxy' is the membrane shear stress. The considered options are as follows: 'sigx' only, 'sigy' only, 'tauxy' only, and all the possible combinations of these three stress components, including 'all-stress' option when all the three stress components are considered.

Some results are presented in Fig. 9, namely: critical force values and buckled shapes, all of them being first buckling modes, calculated by constraining deformations into the pure L space. As the results suggest, various buckling behaviour modes can be achieved depending on the considered stress components. (More precisely: all the stress components are considered in the first-order solution, but the second-order effect of a certain stress is considered or disregarded.)

If the load is acting at the top flange, the middle part of the web is in (transverse) compression, and for this geometry this transverse compression is the governing effect, resulting in a buckling phenomenon typically referred to as 'web crippling'. When the transverse stresses are considered only ('sigy' option), the behaviour is very similar to the 'all-stress'. However, even if these transverse stresses are not considered, buckling is still possible due to either the longitudinal normal stresses or to shear stresses. In these latter cases the buckled shapes are the ones that are typical for the 'plate buckling' of a web in bending, or 'shear buckling' of a web.

When the transverse force is acting at the bottom flange, the middle part of the web is in (transverse) tension, therefore crippling of the middle part of the web does not occur. (In the 'sigy' option there is still buckling solution, but in this case web-crippling-like phenomenon takes place at the supports, and at a much higher load level.)

The load position has little effect on the distribution of the longitudinal normal stresses and on the shear stresses, that is why the buckling patterns and critical values are little affected by the load position in the 'sigx' and 'tauxy' options. The 'all-stress' solution however is greatly dependent on the load position: in the 'top' option the 'all-stress' solution is dominantly a web crippling, in the 'bottom' position it is a combination of shear buckling and plate buckling (of the compressed, upper part of the web).

F_{cr} = 106.702 kN
top, sigx

F_{cr} = 44.655 kN
top, sigy

F_{cr} = 105.034 kN
top, tauxy

F_{cr} = 40.856 kN
top, all-stress

F_{cr} = 99.335 kN
bottom, sigx

F_{cr} = 725.879 kN
bottom, sigy

F_{cr} = 99.974 kN
bottom, tauxy

F_{cr} = 100.022 kN
bottom, all-stress
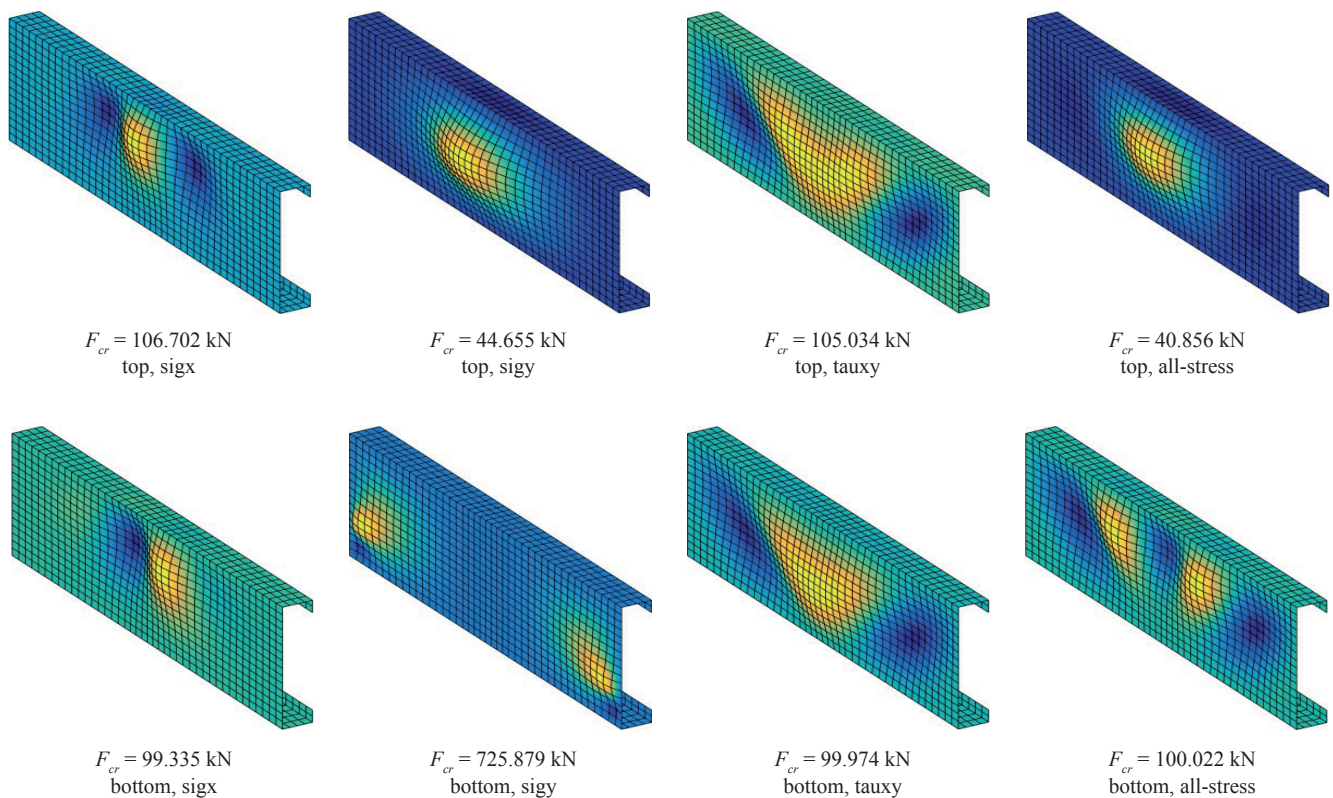
Fig. 9 Buckling mode samples by considering various stress components

4 Conclusions

In this paper a novel finite element method, the so-called constrained (shell) finite element method is discussed. The focus of the paper is on the derivation of local elastic and geometric stiffness matrices, which derivations are completed so that the user can fine-tune the calculations by selecting among multiple options. The derivations are briefly summarized, then numerical examples are provided in comparison (wherever reasonably possible) to results from alternative methods. The results justify the newly derived stiffness matrices as well as demonstrate the effect of various options. The numerical results suggest that it might be practically useful to analyse the effect of the stress components even within a specific deformation space. Though more research is needed in this area, the first results show that, for example, classic 'plate buckling', 'shear buckling' or 'web crippling' can be separated by considering the second-order effect of the longitudinal normal, shear, or transverse normal stresses, respectively, if the analysis is constrained into the local deformation space (to which all these local-plate buckling phenomena belong in a geometric sense). The examples show that the proposed constrained (shell) finite element can beneficially be applied for the analysis (e.g. buckling analysis) of thin-walled members. Without enforcing constraints, the method can be used as an arbitrary shell finite element method. With the implemented multiple options and with the modal decomposition feature, however, it allows a better understanding of the behaviour, as well as it makes possible to have specific buckling solutions in accordance with the needs of the user.

Acknowledgement

References

[1]   AISI S100-2007. North American Specification for the Design of Cold-Formed Steel Structural Members, American Iron and Steel Institute, Washington, DC, USA, 2007. URL: http://www.ce.jhu.edu/cfs/cfslibrary/AISI-S100-07%20Specification.pdf

[2]   EN 1993-1-3:2006, Eurocode 3, Design of Steel Structures, Part 1-3: General rules, Supplementary rules for cold-formed members and sheeting. URL: https://law.resource.org/pub/eu/eurocode/en.1993.1.3.2006.pdf

[3]   Schardt, R. „Verallgemeinerte Technische Biegetheorie. Lineare Probleme." Springer Verlag, Berlin, Heidelberg, 1989. DOI: 10.1007/978-3-642-52330-4

[4]   Gonçalves, R., Ritto-Corrêa, M., Camotim. D. „A new approach to the calculation of crosss-section deformation modes in the framework of generalized beam theory." Computational Mechanics. 46(5), pp. 759–781. 2010. DOI: 10.1007/s00466-010-0512-2

[5]   Silvestre, N. „Generalised beam theory to a nalyse the buckling behaviour of circular cylindrical shells and tubes." Thin-Walled Structures, 45 (2), pp. 185–198. 2007. DOI: 10.1016/j.tws.2007.02.001

[6]   Ádány, S., Schafer, B. W. „Buckling mode decomposition of single-branched open cross-section members via finite strip method: derivation." Thin-Walled Structures, 44 (5), pp. 563–584. 2006. DOI: 10.1016/j.tws.2006.03.013

[7]   Ádány, S., Schafer, B. W. „Buckling mode decomposition of single-branched open cross-section members via finite stripmethod: application and examples." Thin-Walled Structures. 44 (5), pp. 585–600. 2006. DOI: 10.1016/j.tws.2006.03.014

[8]   Schafer, B.W., Ádány, S. „Buckling analysis of cold-formed steel members using CUFSM: Conventional and constrained finite strip methods." In: 18th International Specialty Conference on Cold-Formed Steel Structures: Recent Research and Developments in Cold-Formed Steel Design and Construction. Orlando, FL; United States, Oct. 26-27. 2006.

[9]   Ádány, S., Schafer, B. W. „A full modal decomposition of thin-walled, single-branched open cross-section members via the constrained finite strip method." Journal of Constructional Steel Research.64 (1), pp. 12–29. 2008. DOI: 10.1016/j.jcsr.2007.04.004

[10] Ádány, S., Schafer, B. W. „Generalized constrained finite strip method for thin-walled members with arbitrary cross-section: Primary modes." Thin-Walled Structures. 84, pp. 150–169. 2014. DOI: 10.1016/j.tws.2014.06.001

[11] Ádány, S., Schafer, B. W. „Generalized constrained finite stripmethod for thin-walled members with arbitrary cross-section: Secondarymodes, orthogonality, examples. Thin-Walled Structures, 84, pp. 123–133. 2014. DOI: 10.1016/j.tws.2014.06.002

[12] Ádány, S. „Shell element for constrained finite element analysis of thin-walled structural members." Thin-WalledStructures. 105, pp. 135–146. 2016. DOI: 10.1016/j.tws.2016.04.012

[13] Ádány, S. „Constrained finite element method: demonstrative examples on the global modes of thin-walled members. In: Proceedings of theTwenty-Second International Specialty Conference on Cold-Formed Steel Structures. (LaBoube, R. A., Yu, W. W. (Eds.)) St. Louis, Missouri, USA, Nov. 5-6. 2014. pp. 67-82.

[14] Ádány, S. „Constrained finite element method for the modal analysis of thin-walled members with holes." In: Structural Stability Research Council Annual Stability Conference 2016. Orlando, Florida, USA, Apr. 12-15. 2016.

[15] Ádány, S., Visy, D., Nagy, R. „Buckling solutions for thin-walled members by using the constrained finite element method: demonstrative examples." In: Proceedings of the International Colloquium on Stability and Ductility of Steel Structures, SDSS 2016. (Dubina, D., Ungureanu, V. (Eds.))Timisoara, Romania, May 30-Jun. 2016. pp. 51-58.

[16] Visy, D., Ádány, S. „Local stiffness matrices for the semi-analytical finite strip method in case of various boundary conditions." Periodica Polytechnica Civil Engineering. 58(3), pp. 187–201, 2014. DOI: 10.3311/PPci.7339

[17] Ádány, S. „Global buckling of thin-walled simply supported columns: Analytical solutions based on shell model." Thin-Walled Structures. 55, pp. 64–75. 2012. DOI: 10.1016/j.tws.2012.02.002

[18] Ádány, S., Visy, D. „Global buckling of thin-walled simply supported columns: Numerical studies." Thin-Walled Structures. 54, pp. 82–93, 2012. DOI: 10.1016/j.tws.2012.02.001

[19] ANSYS, Inc. ANSYS ®Mechanical, Release 17.1.

[20] Ádány, S. „Flexural buckling of simply-supported thin-walled columns with consideration of membrane shear deformations: Analytical solutions based on shell model." Thin-Walled Structures. 74, pp. 36–48. 2014. DOI: 10.1016/j.tws.2013.09.014